Electronic Supplementary Information

Giant reversible nanoscale piezoresistance at room temperature in Sr_2IrO_4 thin films

Neus Domingo,[1,*] *Laura López-Mir,*[1,2]*Markos Paradinas,*[2] *Vaclav Holy,*[3]*Jakuv Železný,*[4] *Di Yi,*[5]*SiriyaraJ. Suresha,*[6] *Jian Liu,*[6,7]*Claudy Rayan Serrao,*[5] *Ramamoorthy Ramesh,*[5,6,7] *Carmen Ocal,*[2] *Xavi Martí,*[1,4,8♠] *Gustau Catalán.*[1,9,♣]

[1] ICN2-Institut Català de Nanociència i Nanotecnologia, Campus UniversitatAutònoma de Barcelona, 08193 Bellaterra, Spain

[2] ICMAB, Institut de Ciència de Materials de Barcelona (CSIC), Campus UniversitatAutònoma de Barcelona, 08193 Bellaterra, Spain

[3] Department of Condensed Matter Physics, Faculty of Mathematics and Physics, Charles University, 12116 Praha 2, Czech Republic

[4] Institute of Physics ASCR, v.v.i., Cukrovarnická 10, 162 53 Praha 6, Czech Republic

[5] Department of Materials Science and Engineering, University of California, Berkeley, California 94720, USA

[6] Materials Sciences Division, Lawrence Berkeley National Laboratory, Berkeley, California 94720, USA

[7] Department of Physics, University of California, Berkeley, California 94720, USA

[8] IGS Research, C/ La Coma, Nave 8, 43140 La Pobla de Mafumet (Tarragona), Spain

[9] ICREA - Institució Catalana de Recerca i EstudisAvançats, Barcelona

I. Sample synthesis and characterization

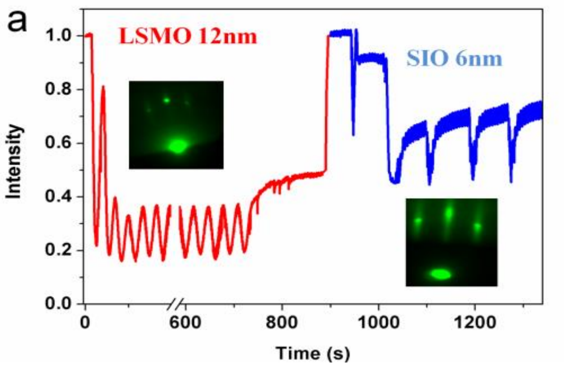

FIG S1: Oscillations of the intensity collected by the Reflection high-energy electron diffraction (RHEED) monitor during the growth of the SIO/LSMO heterostructure. Photographs (inset) show an illustrative RHEED pattern at each step of the fabrication process.

The heterostructure is deposited by pulsed laser deposition (PLD) assisted by reflection high-energy electron diffraction (RHEED). Before the growth, the $SrTiO_3$ (STO) substrate was wet-etched with buffered HF acid, followed by a thermal annealing process, which results in a TiO_2 terminated atomic flat topmost surface. $La_{0.7}Sr_{0.3}MnO_3$ (LSMO) and Sr_2IrO_4 (SIO) were grown epitaxially on the STO substrates from the stoichiometric targets at a laser energy density of ~1.5 J/cm^2 and a repetition rate of 1 Hz. LSMO is grown at 700 °C and 150 mTorr partial oxygen pressure while SIO is grown at 800 °C and 1mTorr. During the deposition, the RHEED intensity oscillations were collected and are shown in Fig. S1. The data indicate a layer by layer growth for each material in both samples. After the growth, the samples were cooled to room temperature in 760 Torr oxygen ambient at a rate of 5°C.

The smooth outermost surface of the heterostructure is revealed by atomic force microscopy (AFM) images as shown in Fig. S2a. The root-mean square surface roughness is below one unit cell (i.e., in the angström range). X-ray diffraction rocking curves for LSMO and SIO, measured at the peak positions in data shown in Fig. S2b, present a full width at half maximum of 0.05° (Fig. S2c). Reciprocal space maps demonstrate a fully epitaxial growth of SIO and LSMO (Fig. S2d). The azimuthal location of the SIO (2 0 24) peaks indicates that the in-plane epitaxial relationship is [100]STO//[100]LSMO//[110]SIO.

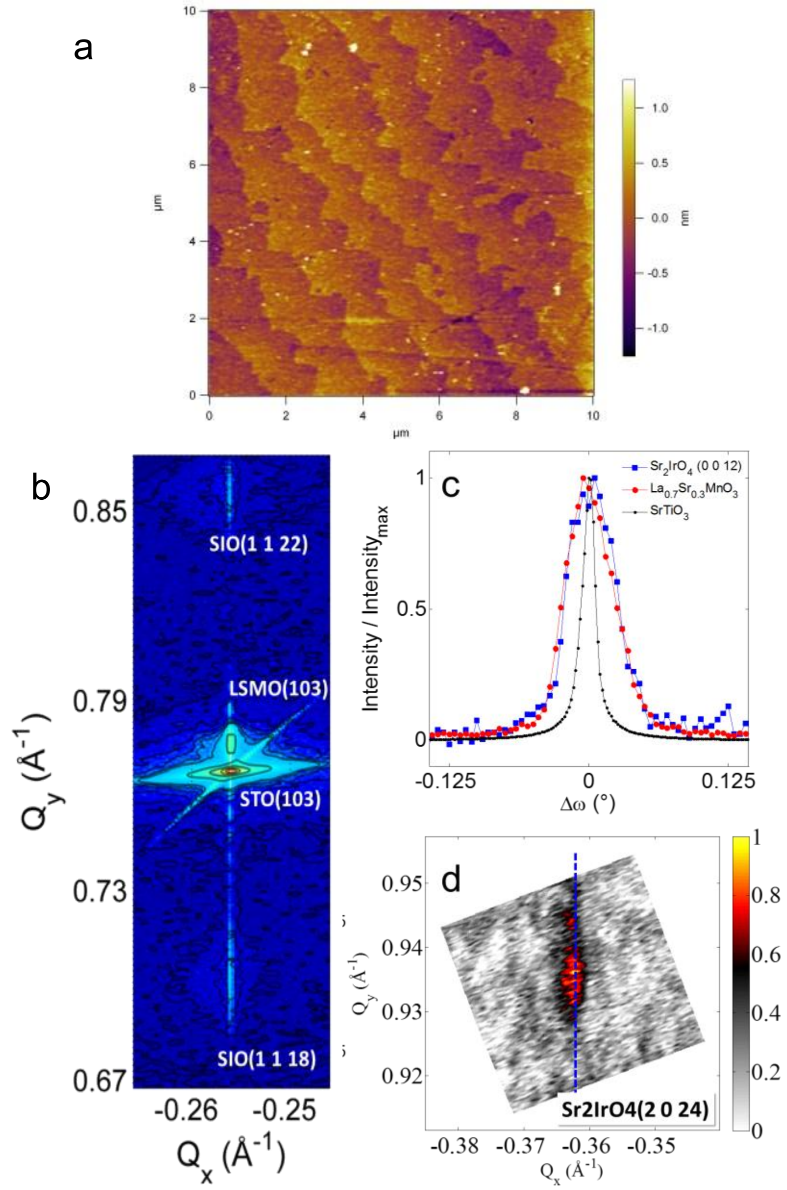

FIG S2:a. Topmost surface topography of the SIO/LSMO stack obtained by atomic force microscopy. **b.** X-ray diffraction pattern of the heterostructure showing the fully epitaxial stacking of SIO on top of bottom ferromagnetic electrode LSMO, on the STO substrate. Labels signal the Miller indexes of the observed reflections. **c.** X-ray diffraction rocking curves around the STO(002), LSMO(002) and SIO(00 12) reflections. **d.** Reciprocal space mapping around the SIO(2 0 24) reflection. Dashed blue line denotes the horizontal location of the STO(114) substrate peak (not shown).

II. Stability of surface isolating state after pressure. Influence of tip coating material.

In Fig. S3, we show the C-AFM map after performing different I(V_{tip}) curves at different force set points in the dashed circles, from loads of 200 nN to 5 μN, in steps of 200 nN (25 points map). No signal of irreversible permanent current is observed after applying the loads point by point, meaning that the increase of conductivity cannot be produced by the appearance of pressure induced defects or breakthroughs.

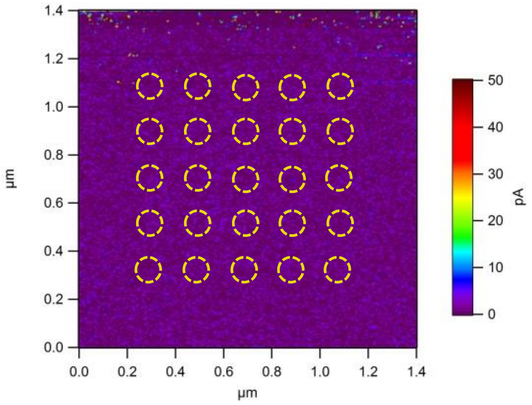

FIG S3: C-AFM image with an applied voltage of 500 mV measured with a load of 200 nN, after several I(V) curves characterization under different loads in the areas marked with dashed circles. No signal of permanent change in resistivity is observed.

In order to account for the influence of the tip coating on the measurements, different tips were used to perform characterization of resistance *vs* load. Results shown in Figure S4 reflect the intrinsic difference in conductivity due to different coatings. We note that the coating provides a resistance in series with the sample resistance in the CPP configuration, inducing a slight offset in the measured total resistance values for each probe as well as currents with different absolute magnitude. On top of that, the influence on the tip radius is also observed. The nominal tip radius of the different probes are R_{tip}(PtSi) ~ 20 nm <R_{tip} (PtIr) ~50 nm <R_{tip} (Diamond) ~150 nm. Local pressure values induced by such tips would then scale in inverse order, thus leading to the need of smaller loads to induce the same strain locally.

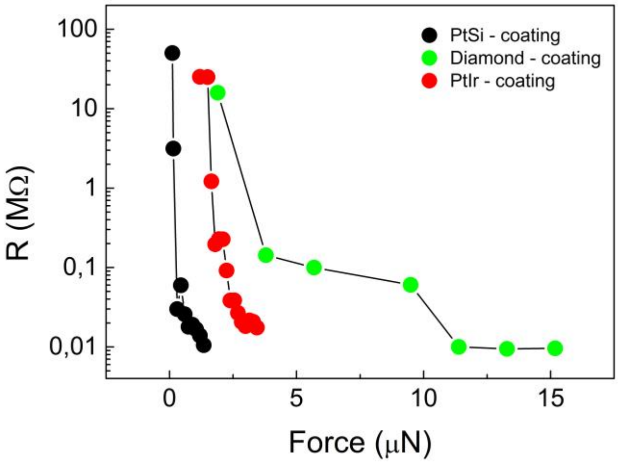

FIG S4: Total resistance obtained from the slope of I(V) curves under different loads for different types of tip materials and tip radius.

III. Calculation of effective resistivity. Tip-sample mechanical coupling and geometrical effects.

Fig S5a shows a force versus distance curves up to a maximum of 7 μN on the SIO epitaxial layer. A tip of Nanosensors CDT-NCH with k = 55 N/m,as calculated by Sader method[1], was used. The slope of the curve is constant over all the extension of the z-piezo raw positioner, indicating a pure elastic non-indentation model for the tip-sample contact. Moreover, adhesion forces are also negligible, thus supporting the application of the Hertz model for the tip-sample contact area approximation.

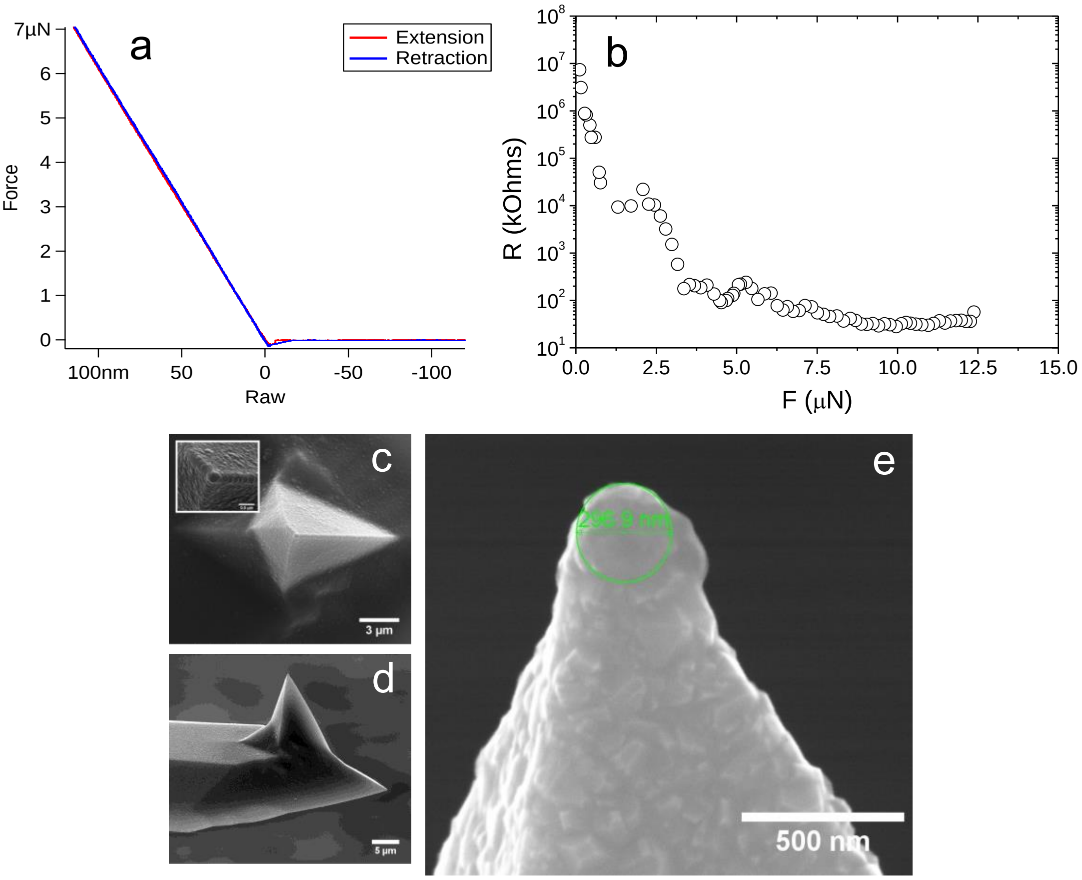

FIG S5, a Force curve of SIO epitaxial layer with a Nanosensor CDT-NCH tip with a calculated k = 55 N/m. **b**, Restistance values obtained from the 3D conductive maps as a function of the measured force. **c**,**d** and **e,** show SEM images of the corresponding tip after the measurements. Spherical shaped tip is confirm to prevail after the measurements, and tip radius can be aproximated from the SEM images to be about 150 nm.

Figure S5 b shows the original resistance vs force data obtained from the 3D conductive measurements. On these grounds, we can calculate the effective contact radius a for each applied force, following the Hertz elastic contact model as:

$$a = \left(\frac{3}{4}\frac{F \cdot r_{tip}}{E^*}\right)^{1/3} \qquad \text{(Eq. 1)}$$

where E^* is the Young elastic modulus and r_{tip} is taken from the SEM images. With these values, we can determine the mean contact pressure exerted on a column of SIO, as:

$$P_m = \left(\frac{4E^*}{3\pi}\right)\frac{a}{r_{tip}} \qquad \text{(Eq. 2)}$$

and estimate an effective resistivity value ρ_{eff} for different loading conditions on the basis of the normalization of the total resistance value R by the effective contact area, as:

$$\rho_{eff}(P_m) = R \cdot \frac{\pi a^2}{d - {a^2}/{r_{tip}}} \qquad \text{(Eq. 3)}$$

where we also consider the reduction on the thickness of the film by the deformation depth

$$\delta = \frac{a^2}{r_{tip}} \qquad \text{(Eq. 4)}$$

IV. Calculation of elastic constants.

We calculated the elastic constants of SIO using an all-electron full potential DFT code WIEN2k[2] with the PBE-GGA exchange correlation potential and the Elastic package.[3] We used the so called energy approach, in which the elastic constants are found by taking second derivative of total energy with respect to particular strains. To find the energy as a function of strain, we calculated total energy for several strained structures and fitted the results to a cubic polynomial.

We considered strains ranging from -2% to 2% and for each strain we relaxed the atomic positions. As a starting point we did not use the experimental lattice constants, instead we used lattice constants found by energy minimization. The Brillouin zone was sampled by a set of 7x7x7k points and the size of the basis was given by RK=6.5. We included neither spin orbit coupling nor LDA+U, as a result of that in our calculation SIO is wrongly identified as a non magnetic metal[4]. This calculation should, therefore, be understood only as a rough approximation of the elastic constants.

Elastic constants	
c11	217.3876 GPa
c12	151.5501 GPa
c13	99.9247 GPa
c33	286.1155 GPa
c44	44.6019 GPa
c66	72.0158 GPa

V. Simulation of uniaxial stress

In order to quantify the mechanical pressure exerted onto the thin film, we apply the Hertzian contact model. It describes a system of a spherical indenter pressing against an elastic flat specimen neglecting adhesive forces. According to this model, an AFM tip exerts the normal stress σ_S at the free sample surface at $z = 0$

$$\sigma_S(x,y) = \begin{cases} \frac{3F}{2\pi R^2}\sqrt{1-\frac{x^2+y^2}{R^2}} & \text{for} \sqrt{x^2+y^2} < R \\ 0 & \text{elsewhere} \end{cases} \quad \text{(Eq.5)}$$

where F is the applied force and R is the radius of the contact area. The deformation of the sample caused by this surface stress is calculated numerically, taking into account the equilibrium conditions for the layer and the semi-infinite substrate. Both conditions have the same form

$$\frac{\partial \sigma_{jk}^{(M)}}{\partial x_k} = C_{jkmn}^{(M)} \frac{\partial^2 u_m^{(M)}}{\partial x_k \partial x_n} = 0, \; j,k,m,n = x,y,z, \; M = \text{layer, substrate} \quad \text{(Eq.6)}$$

whereσ_{jk} is the stress tensor, u_j are the components of the displacement vector, and C_{jkmn} are the elastic constants in the 3x3x3x3 notation. The boundary conditions at the free surface z = 0 are $\sigma_{xz} = \sigma_{yz} = 0$; $\sigma_{zz} = \sigma_S\,(x,\,y)$, while at the buried layer-substrate interface I we assume the continuity of the displacement components $u^{(\text{layer})}(r)|_I = u^{(\text{substrate})}(r)|_I$ and the continuity of the jz components of the stress tensor$\sigma_{jz}^{(\text{layer})}(r)|_I = \sigma^{(\text{substrate})}(r)_{jz}|_I$, $j = x,y,z$. In the semi-infinite substrate, we assume $\lim_{z\to\infty} u^{(\text{substrate})}(r) = 0$. We use the two-dimensional Fourier transformation along the in-plane coordinates x, y

$$u(r) = \frac{1}{4\pi^2}\int \mathrm{d}^2k\, u^{FT}(k,z) e^{ik,x}, x \equiv (x,y) \quad \text{(Eq.7)}$$

which converts the partial differential equations (Eq. 6) into two ordinary linear differential equations for $u^{\text{FT(layer)}}(k,z)$, $u^{\text{FT(substrate)}}(k,z)$; these equations are solved by standard methods, taking into account the boundary conditions above.

1. Sader, J. E.; Chon, J. W. M.; Mulvaney, P. *Review of Scientific Instruments* **1999,** 70, (10), 3967-3969.

2. P. Blaha; K. Schwarz; G. Madsen; D. Kvasnicka; Luitz, J., *WIEN2k, an augmented plane wave + local orbitals program for calculating crystal properties*. Techn.Universität Wien 2001.

3. Reshak, A. H.; Jamal, M. *Journal of Alloys and Compounds* **2012,** 543, 147 - 151.

4. B. Kim; Hosub Jin; S. Moon; J.-Y. Kim; B.-G. Park; C. Leem; Jaejun Yu; T. Noh; C. Kim; S.-J. Oh; J.-H. Park; V. Durairaj; G. Cao; Rotenberg, E. *Physical Review Letters* **2008,** 101, 076402.